

Pressure effects on charge-ordering transitions in Perovskite manganites

Y. Moritomo,* H. Kuwahara, and Y. Tomioka
Joint Research Center for Atom Technology, Tsukuba 305, Japan

Y. Tokura
Joint Research Center for Atom Technology, Tsukuba 305, Japan
and Department of Applied Physics, University of Tokyo, Tokyo 113, Japan
 (Received 3 November 1995; revised manuscript received 15 October 1996)

Effects of chemical and external pressures have been investigated on the two types of charge-ordering (CO) systems of perovskite manganites with the use of single-crystal specimens: One is $\text{Nd}_{1-x}\text{Sr}_x\text{MnO}_3$ with moderate CO instability occurring only near $x=1/2$ and the other is $\text{Pr}_{1-x}\text{Ca}_x\text{MnO}_3$ with stronger CO instability extending over a wide x region $0.3 \leq x \leq 0.7$. We have partially substituted the Nd ions of $\text{Nd}_{1/2}\text{Sr}_{1/2}\text{MnO}_3$ with larger La ions or applied external pressure on them with the aim of destabilizing the CO state via an increase of the $3d$ -electron hopping interaction. An electronic phase diagram relevant to the CO transition was derived for $(\text{Nd}_{1-z}\text{La}_z)_{1/2}\text{Sr}_{1/2}\text{MnO}_3$ by such a control of the one-electron bandwidth (W). With an increase of W , the enhanced ferromagnetic double-exchange interaction increases the Curie temperature (T_C) and suppresses the charge-ordered state with a concomitant antiferromagnetic charge-exchange-type spin ordering (AF-CE). In a narrow window of z ($0.4 \leq z \leq 0.6$) or in the pressurized state for $z=0.4$, another type of antiferromagnetic (perhaps the A type) phase replaces the AF-CE state. Application of external pressure and resultant enhanced carrier itineracy suppresses the CO transitions also for $\text{Pr}_{1-x}\text{Ca}_x\text{MnO}_3$. For the $x=0.30$ crystal, application of pressure induces a metallic phase from the low-temperature side in the charge-ordered insulating phase. The pressure-temperature phase diagrams relating to the CO transition or the concurrent insulator-to-metal transition were shown to scale well with the magnetic-field-temperature phase diagrams. [S0163-1829(97)06511-9]

I. INTRODUCTION

Electronic properties of correlated electron systems, especially near the insulator-metal (IM) phase boundary, are sensitive to the magnitude of the one-electron bandwidth (W). In transition-metal oxides with an orthorhombically distorted perovskite structure $R\text{MO}_3$, where R and M are, respectively, the rare-earth and transition-metal ions, the W value can be controlled by varying the M -O- M bond angle through change of the average ionic radius of R .^{1,2} Torrance *et al.*¹ derived an electronic phase diagram for $R\text{NiO}_3$ ($M=\text{Ni}$) with systematic variation of the ionic radius of R . The critical temperature (T_{MI}) for the metal-to-insulator transition in $R\text{NiO}_3$ decreases with an increase of the ionic radius or an increase of the W value and eventually the insulating phase disappears for $R=\text{La}$. Similarly to the chemical control of the M -O- M bond angle (*chemical* pressure effect), the W value can be increased by the application of an external pressure through contradiction of the M -O bond length or straightening of the M -O- M bond angle.³⁻⁶ Compared to the chemical pressure, the external pressure is a clean perturbation and is free from the randomness of the potential introduced by chemical substitution. However, the controllable range of W by the external pressure is narrower than that by the chemical substitution. Then, a combination study of the chemical and external pressures will give us important information on the electronic nature of correlated electron system.

Perovskite-type manganites $R_{1-x}A_x\text{MnO}_3$ become a conducting ferromagnet with hole doping (x). The ferromagnetic interaction or the double-exchange (DE) interaction in

these compounds is mediated by the itinerant e_g carriers,^{7,8} which magnetically couple with the local t_{2g} spins via the on-site exchange interaction (Hund's-rule coupling J_H). The doped manganites show a large negative magnetoresistance (MR) around the Curie temperature (T_C), which has been ascribed to alignment of the local t_{2g} spins and reduction of the spin scattering of the e_g carriers by a magnetic field. The MR behavior of the manganites with a relatively large W value (e.g., $\text{La}_{1-x}\text{Sr}_x\text{MnO}_3$) is well reproduced by a simplified DE model,^{9,10} which considers merely the transfer interaction of the itinerant e_g carriers and the on-site ferromagnetic interaction J_H between the e_g electron and local t_{2g} spin.¹¹ On the other hand, Millis *et al.*¹² have argued that the effect of the Jahn-Teller interaction inherent to the MnO_6 octahedron is essential to reproduce the temperature variation of the resistivity near T_C (in particular, the semiconducting behavior above T_C) as well as the "colossal" value of MR in the low-doped region or for the small- W system such as $\text{La}_{1-x}\text{Ca}_x\text{MnO}_3$.

In addition to the ferromagnetic transition, the doped manganites often undergo a phase transition to a charge-ordered state, in which the nominally Mn^{3+} and Mn^{4+} species show a real-space ordering in the crystal, in the case where the doping level (x) is near a commensurate value ($=1/2$).¹³⁻¹⁶ The charge-ordering (CO) transition accompanies an appreciable change in the lattice parameters.^{13,16,17} These CO transitions can be classified into two types (referred to hereafter as type I and type II). In type I, the charge-ordered state emerges with the concomitant antiferromagnetic spin ordering in the metallic ferromagnetic phase

($T_{CO} < T_C$, T_{CO} being the critical temperature for the CO transition) in the case where the CO instability is not so strong. $\text{Nd}_{1/2}\text{Sr}_{1/2}\text{MnO}_3$ (Ref. 13) is classified into this type (type I), which becomes a conducting ferromagnet below $T_C = 250$ K and then an antiferromagnetic [charge-exchange (CE)-type] charge-ordered insulator below $T_{CO} \approx 158$ K. When the CO instability is further enhanced in a narrower- W system, the charge-ordered phase emerges at higher temperature (virtually exceeding T_C) and the ferromagnetic metallic (FM) phase is no longer present (type II). In this case, the antiferromagnetic transition temperature (T_N) is usually lower than T_{CO} . $\text{Pr}_{1-x}\text{Ca}_x\text{MnO}_3$ is a prototypical example for type II. The CO phase extends over a wide range of hole concentration ($0.3 \leq x \leq 0.7$) in $\text{Pr}_{1-x}\text{Ca}_x\text{MnO}_3$, and no FM phase appears in any x region at zero field.^{16,18,19}

An external magnetic field has significant effects not only on the ferromagnetic transition but on the charge-ordering transition. This is because the effective transfer integral (t) of the e_g carriers strongly depends on alignment of the t_{2g} spins⁷

$$t = t_0 \cos(\Delta\theta/2), \quad (1)$$

where t_0 is the bare transfer integral without spin scattering and $\Delta\theta$ is the relative angle of the neighboring t_{2g} spins. An external magnetic field forcibly aligns the t_{2g} spins ($\Delta\theta \rightarrow 0$), enhances the carrier itineracy, and modifies the CO state. In an extreme case, the application of a magnetic field destroys the CO state and induces a FM state from the low-temperature side, as exemplified in $\text{Pr}_{1-x}\text{Ca}_x\text{MnO}_3$.^{18,19} Similarly to the magnetic field that directly acts on the spin state, external or chemical pressure is expected to enhance the ferromagnetic DE interaction²⁰ through an increase of the bare transfer integral (t_0) and hence modifies the charge-ordered state.

In this paper, we report on the effects of chemical and external pressure on the two types of CO systems: $\text{Nd}_{1-x}\text{Sr}_x\text{MnO}_3$ ($x=1/2$) with moderate CO instability (type I) and $\text{Pr}_{1-x}\text{Ca}_x\text{MnO}_3$ ($0.30 \leq x \leq 0.50$) with strong CO instability (type II). In the former system, we can control the W value by partially replacing the Nd^{3+} ions with larger La^{3+} ions as well as by applying external pressure. We have derived an electronic phase diagram for $(\text{Nd}_{1-z}\text{La}_z)_{1/2}\text{Sr}_{1/2}\text{MnO}_3$ as a function of the averaged ionic radius (or z), which is a good measure of the one-electron bandwidth (W) of the e_g band. With increase of W (or increase of z), the enhanced ferromagnetic DE interaction suppresses the charge-ordered state with antiferromagnetic (AF) CE-type spin ordering and eventually the charge-ordered state disappears above $z=0.6$. In a narrow window of z ($0.4 \leq z \leq 0.6$), another type of antiferromagnetic (perhaps the A type, AF-A) phase replaces the AF-CE state as a possible consequence of the subtle balance between the competing interactions. In the case of $\text{Pr}_{1-x}\text{Ca}_x\text{MnO}_3$, pressure-enhanced carrier itineracy also suppresses the CO transition and enlarges the high-temperature low-resistive state. For the $x=0.30$ crystal, we observed an IM transition under pressures, which can be interpreted in terms of collapse of the CO. Similar pressure-induced IM transition was recently reported by Hwang *et al.*³ for a polycrystalline sample of $\text{Pr}_{1-x}\text{Ca}_x\text{MnO}_3$ ($x=0.3$). We compare these pressure-

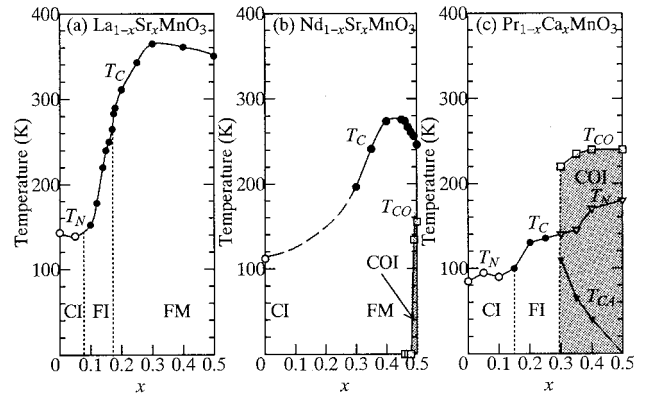


FIG. 1. Electronic phase diagrams for perovskite manganites: (a) $\text{La}_{1-x}\text{Sr}_x\text{MnO}_3$ (cited from Ref. 10), (b) $\text{Nd}_{1-x}\text{Sr}_x\text{MnO}_3$ (cited from Ref. 21 and present work), and (c) $\text{Pr}_{1-x}\text{Ca}_x\text{MnO}_3$ (cited from Refs. 16 and 19). The abbreviations represent spin-canted insulating (CI), ferromagnetic insulating (FI), ferromagnetic metallic (FM), and charge-ordered insulating (COI) states, respectively. T_C , T_N , T_{CO} , and T_{CA} stand ferromagnetic, antiferromagnetic, and charge-ordering and spin-canting transition temperatures, respectively.

induced phenomena observed for single crystals of $\text{Pr}_{1-x}\text{Ca}_x\text{MnO}_3$ ($0.3 \leq x \leq 0.5$) with the effects of an external magnetic field from a unified viewpoint of the CO instability and present an empirical scaling relation between the effects of pressure and magnetic field.

II. ELECTRONIC PHASE DIAGRAM

First, let us survey the electronic phase diagrams for perovskite manganites as shown in Fig. 1(a), $\text{La}_{1-x}\text{Sr}_x\text{MnO}_3$;¹⁰ Fig. 1(b), $\text{Nd}_{1-x}\text{Sr}_x\text{MnO}_3$;²¹ and Fig. 1(c), $\text{Pr}_{1-x}\text{Ca}_x\text{MnO}_3$.^{16,19} As the averaged ionic radius of the perovskite A site decreases from (La,Sr) to (Pr,Ca) through (Nd,Sr), the orthorhombic distortion of the GdFeO_3 type increases.² As a result, the reduced Mn-O-Mn bond angle suppresses the itineracy of the e_g carriers. This means that other electronic instabilities, such as the CO and antiferromagnetic superexchange interactions, which compete with the ferromagnetic DE interaction, may become dominant in specific x and temperature regions.

The phase diagram for $\text{La}_{1-x}\text{Sr}_x\text{MnO}_3$ [Fig. 1(a)] is a canonical one for the DE system.¹⁰ The Jahn-Teller distorted state ($x \leq 0.1$) undergoes a phase transition to a spin-canted insulating phase. With further doping, the FM phase appears below T_C . T_C steeply increases with x up to $x=0.3$ and then saturates. A ferromagnetic insulating (FI) phase is present in a fairly narrow x region ($x=0.10-0.17$) in which the e_g carriers are subject to localization but can still mediate the ferromagnetic interaction between the neighboring sites and realize the ferromagnetic state in a bond-percolation manner. Such a FI phase expands as the averaged ionic radius decreases: The low-temperature ferromagnetic phase is insulating up to $x=0.3$ for $\text{Pr}_{1-x}\text{Ca}_x\text{MnO}_3$, as seen in Fig. 1(c).

In the case of $\text{Nd}_{1-x}\text{Sr}_x\text{MnO}_3$ [Fig. 1(b)] with a narrower

one-electron e_g band, T_C is suppressed as compared with $\text{La}_{1-x}\text{Sr}_x\text{MnO}_3$ and begins to drop with hole doping beyond $x \approx 0.4$. In the immediate vicinity of $x = 0.5$, a charge-ordered insulating (COI) phase sets in below $T_{\text{CO}} (< T_C)$. The CO transition at $x = 0.5$ ($T_{\text{CO}} = 158$ K) accompanies a ferromagnetic-antiferromagnetic transition¹³ and the low-temperature spin structure is known to be of the CE type as in $\text{La}_{1-x}\text{Ca}_x\text{MnO}_3$.¹⁵ The transition also accompanies a significant change in the lattice parameters: In the orthorhombic ($Pbnm$) setting, a and b lengthen by ≈ 0.5 – 0.9 % and the c shrinks by ≈ 1.5 %.¹³ The charge-ordered state is observed only in a limited x region and disappears below $x = 0.48$. Recently, Kawano *et al.*²² performed neutron scattering measurement and found that the low-temperature spin structure at $x = 0.55$ is not of the CE type but of the layered type (A type) along the $[0\ 0\ 1]$ direction in the $Pbnm$ setting and that no sign of CO is observed.

For $\text{Pr}_{1-x}\text{Ca}_x\text{MnO}_3$ [Fig. 1(c)] with a further reduced W , the charge-ordered phase extends over a wide range of hole concentration ($x \geq 0.3$) below 220–240 K and no FM phase shows up in any x region.¹⁹ In the charge-ordered phase of this compound, there are successive magnetic transitions to a spin-collinear antiferromagnetic phase (at T_N) and to a spin-canted antiferromagnetic phase (at T_{CA}). The observed variation of the transition temperatures T_N and T_{CA} with x may be interpreted in terms of the partial revival of the DE carriers in the charge-ordered phase: The CO pattern is always $(1/2, 1/2, 0)$ in the pseudocubic setting irrespective of x and hence the deviation of x from $x = 1/2$ produces extra carriers that modify the spin structure as observed.¹⁶ This is in sharp contrast to the case of $\text{Nd}_{1-x}\text{Sr}_x\text{MnO}_3$, in which a small number of extra carriers (0.02–0.05 per Mn site) appear to destroy the charge-ordered state at $x \approx 0.5$.

III. EXPERIMENT

A. Crystal growth

Crystals of the doped manganites were grown by the floating-zone method at a feeding speed of 7–9 mm/h for $(\text{Nd}_{1-z}\text{La}_z)_{1/2}\text{Sr}_{1/2}\text{MnO}_3$ ($0 \leq z \leq 1$) and $\text{Nd}_{1-x}\text{Sr}_x\text{MnO}_3$ ($0.3 \leq x \leq 0.5$) and 3–5 mm/h for $\text{Pr}_{1-x}\text{Ca}_x\text{MnO}_3$ ($0.3 \leq x \leq 0.5$).^{10,19} A stoichiometric mixture of Nd_2O_3 , La_2O_3 , SrCO_3 , Mn_3O_4 , Pr_6O_{11} , and SrCO_3 was ground and calcined three times at 1050 °C for 24 h. Then the resulting powder was pressed into a rod with a size of 5 mm $\phi \times 60$ mm and sintered at 1350 °C for 48 h (Nd-based crystals) or 1200 °C–1300 °C for 48 h (Pr-based crystals). The ingredient could be melted congruently in a flow of air or O_2 using a floating-zone furnace with two incandescent halogen lamps. Results of powder x-ray-diffraction measurement and electron probe microanalysis indicated that the crystals are single phase and show nearly identical compositions to the prescribed ones. In the case of $(\text{Nd}_{1-z}\text{La}_z)_{1/2}\text{Sr}_{1/2}\text{MnO}_3$, the crystal structure is orthorhombic ($Pbnm$, $Z=4$) for $0 \leq z \leq 0.5$ and rhombohedral ($R\bar{3}c$, $Z=2$) for $z \geq 0.6$. In the respective phases, the room-temperature lattice constants monotonically vary with z .

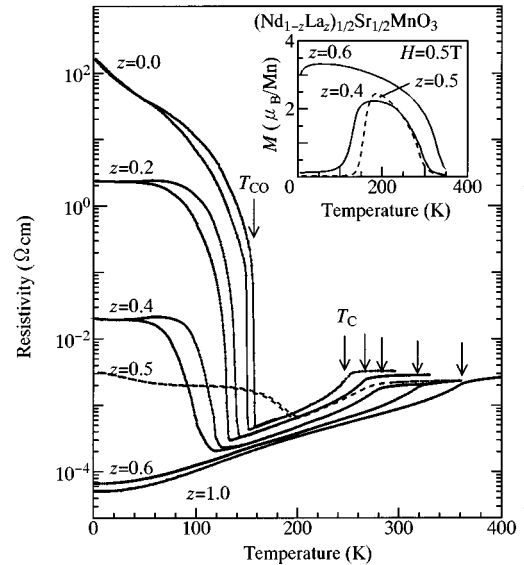


FIG. 2. Temperature dependence of resistivity for $(\text{Nd}_{1-z}\text{La}_z)_{1/2}\text{Sr}_{1/2}\text{MnO}_3$ crystals with varying z value. T_C and T_{CO} represent ferromagnetic temperature and charge-ordering transition temperatures, respectively. The inset shows the temperature dependence of the magnetization (under a field of 0.5 T) for $z = 0.4, 0.5$, and 0.6 , which was measured after cooling down to 5 K in a zero field. A broken curve represents the data for $z = 0.5$.

B. High-pressure experiment

A hydrostatic pressure was obtained with a clamp-type piston cylinder cell. Resistivity (ρ) was measured by the four-probe method using heat-treatment-type silver paint as electrodes. A small piece of crystal ($\sim 0.5 \times 1 \times 2$ mm³) was placed in a sample room, which was filled with silicone oil as a pressure-transmitting medium. The sample temperature was monitored with a copper-constantan thermocouple placed in the sample room and an AuFe(0.07%)-chromel thermocouple attached near the sample room. The pressure values quoted in this paper are those measured at room temperature. We also measured ac susceptibility (χ) under pressures for the purpose of precise determination of T_C .²⁰ A small piece of crystal (~ 10 mg) was placed in a coil (2 mm in diameter and ≈ 10 mm in length), of which inductance was monitored with a LCR meter at a frequency of 1 MHz. Pressure-induced changes in the ρ - T and χ - T curves were reproducible in repeated pressure cycles.

IV. CHARGE-ORDERING TRANSITIONS FOR $\text{Nd}_{1-x}\text{Sr}_x\text{MnO}_3$

A. Pressure control of the CO transition

From a comparison between the phase diagrams for $\text{La}_{1-x}\text{Sr}_x\text{MnO}_3$ and $\text{Nd}_{1-x}\text{Sr}_x\text{MnO}_3$ (Fig. 1), we may expect to investigate the bandwidth dependence of the charge-ordered state (at $x = 1/2$) by using the A -site solid solution systems $(\text{Nd}_{1-z}\text{La}_z)_{1/2}\text{Sr}_{1/2}\text{MnO}_3$ ($0 \leq z \leq 1$). Figure 2 shows the ρ - T curves for $(\text{Nd}_{1-z}\text{La}_z)_{1/2}\text{Sr}_{1/2}\text{MnO}_3$ with various z values. With an increase of W (or an increase of z), the enhanced DE interaction suppresses the CO transition: T_{CO} decreases from $T_{\text{CO}} = 158$ K at $z = 0$ to 120 K at

TABLE I. Space group and lattice parameters for $(\text{Nd}_{1-z}\text{La}_z)_{1/2}\text{Sr}_{1/2}\text{MnO}_3$. T_{CO} and T_N are charge-ordering and Néel temperatures, respectively.

| z | Space group | 300 K (Å) | 200 K (Å) | 100 K (Å) | 30 K (Å) |
|------------------------------|-------------|-------------------------|-------------------|-------------------|-------------------|
| 0.4 $T_{\text{CO}}=120$ K | $Pbnm$ | $a=5.4779(2)$ | $5.4743(2)$ | $5.5171(13)$ | $5.5180(13)$ |
| | | $b=5.4283(2)$ | $5.4320(2)$ | $5.4596(18)$ | $5.4604(20)$ |
| | | $c=7.6539(3)$ | $7.6529(3)$ | $7.5455(15)$ | $7.5456(16)$ |
| 0.5 $T_N=195$ K | $Pbnm$ | $a=5.4846(6)$ | $5.4798(7)$ | $5.5081(4)$ | $5.5093(4)$ |
| | | $b=5.4417(7)$ | $5.4374(7)$ | $5.4595(4)$ | $5.4606(4)$ |
| | | $c=7.6580(8)$ | $7.6441(9)$ | $7.5516(5)$ | $7.5492(5)$ |
| 0.6 | $R\bar{3}c$ | $a=5.4503(3)$ | $5.4485(5)$ | $5.4476(6)$ | $5.4470(7)$ |
| | | $\beta=60.367(3)^\circ$ | $60.228(6)^\circ$ | $60.235(7)^\circ$ | $60.253(8)^\circ$ |

$z=0.4$ and the charge-ordered state disappears above $z=0.6$. In Table I we show the lattice parameters for $(\text{Nd}_{1-z}\text{La}_z)_{1/2}\text{Sr}_{1/2}\text{MnO}_3$ ($z=0.4, 0.5$, and 0.6) at several temperatures. The lattice constants for $z=0.4$ ($T_{\text{CO}}=120$ K) show a large change between 200 K ($>T_{\text{CO}}$) and 100 K ($<T_{\text{CO}}$): a and b expand by $\approx 0.5\text{--}0.8\%$ and c shrinks by $\approx 1.3\%$ perhaps upon the CO transition as observed in $\text{Nd}_{1/2}\text{Sr}_{1/2}\text{MnO}_3$ ($z=0$).¹³ By contrast, no prominent change of the lattice constants is observed for $z=0.6$ apart from the slight thermal shrinkage.

One may notice that the $z=0.5$ sample (indicated by a broken curve in Fig. 2) shows a curious behavior. As seen in the inset of Fig. 2, the ferromagnetic-antiferromagnetic transition shows up as an abrupt disappearance of the ferromagnetic magnetization at T_N . T_N rather increases in going from $z=0.4$ to 0.5 . Furthermore, the ρ - T curve for $z=0.5$ shows an anomaly at T_N , but the ρ value remains fairly low ($\sim 4 \times 10^{-3} \Omega \text{ cm}$) even at sufficiently low temperatures below T_N . These imply that the low-temperature magnetic structure for $z=0.5$ is different from that for $z=0$ (CE type) because the transport property is significantly affected by the spin structure. A good reference may be $\text{Pr}_{1/2}\text{Sr}_{1/2}\text{MnO}_3$ with the nearly corresponding tolerance factor (or the A -site averaged ionic radius), whose low-temperature spin structure is of the layered type (A type) along the $[1\ 1\ 0]$ direction in the $Pbmn$ setting.²² The resistivity for $\text{Pr}_{1/2}\text{Sr}_{1/2}\text{MnO}_3$ remains rather low²³ ($\sim 10^{-2} \Omega \text{ cm}$) at ≈ 5 K, in sharp contrast to the transport properties for $\text{Nd}_{1/2}\text{Sr}_{1/2}\text{MnO}_3$, whose low-temperature spin structure is of the CE type. From this analogy, we speculate that the spin structure for $z=0.5$ is different from the CE type and perhaps the A type. Hereafter, we will refer to this antiferromagnetic phase tentatively as the AF-A phase. The magnetic phase transition for $z=0.5$ accompanies a lattice anomaly similar to the case of $z=0.4$, i.e., elongation of a and b and shrinkage of c (see Table I).

The application of pressure, which also increases the W value, appears to induce a transition from the charge-ordered AF-CE state to the AF-A state. We show in Fig. 3 the pressure dependence of resistivity for $z=0.4$ that shows the CO transition at ambient pressure. (The respective two curves correspond to the cooling and warming runs.) We adopted the minimum position of the ρ - T curve as the phase transition temperature. The transition temperature gradually in-

creases with pressure accompanying a steep reduction of the ρ value. The ρ - T curves at $P=1.1$ and 1.4 GPa for $z=0.4$ show a close resemblance to that for $z=0.5$ at ambient pressure (broken curves), suggesting that the high-pressure (≥ 1 GPa) phase is essentially the same as the AF-A state.

Thus obtained T_C , T_{CO} , and T_N are plotted with open symbols in Fig. 4 as a function of z . The hatched area in the figure represents the thermal hysteresis of T_{CO} and T_N . Among them, T_C under pressure was determined from the temperature variation of the ac susceptibility (χ). In the same figure we also plot the respective transition temperatures obtained under pressures (solid symbols) using the common scaling relation that $\Delta z=0.04P$, where Δz is an effective increment of z and P is in units of GPa. Using the above scaling relation, the obtained pressure data can be presented consistently with the ambient pressure data as a function of z , as shown by eye-guiding curves. With an increase of z , the enhanced DE interaction increases T_C and suppresses T_{CO} . In the region of $0.4 \leq z \leq 0.6$, the AF-A state replaces the AF-CE state and T_C shows an anomalous decrease with z . In the rhombohedral phase ($z \geq 0.6$), no anti-

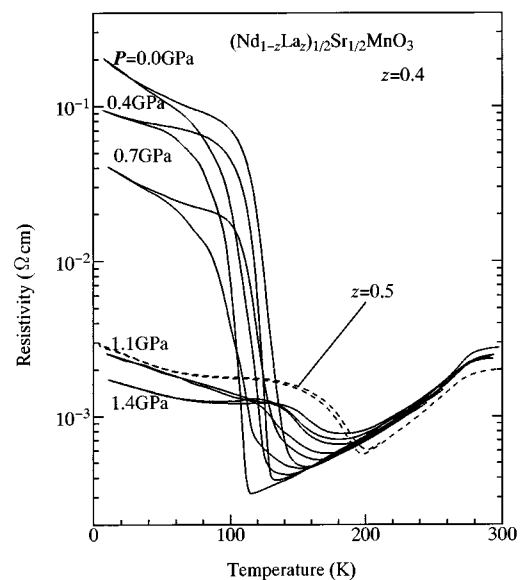


FIG. 3. Pressure dependence of resistivity for $(\text{Nd}_{0.6}\text{La}_{0.4})_{1/2}\text{Sr}_{1/2}\text{MnO}_3$ ($z=0.4$) crystal. A broken curve represents the data for $z=0.5$ at ambient pressure.

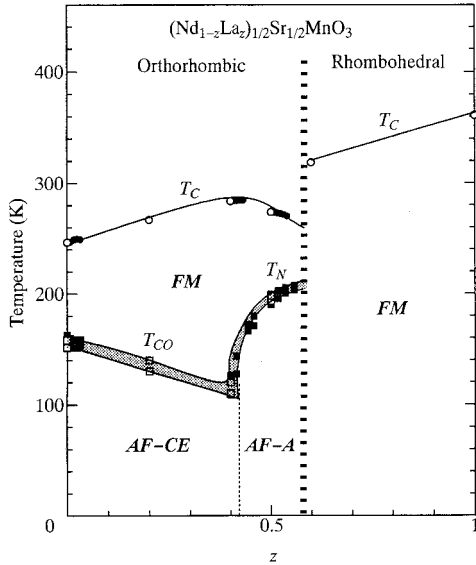


FIG. 4. Electronic phase diagram for $(\text{Nd}_{1-z}\text{La}_z)_{1/2}\text{Sr}_{1/2}\text{MnO}_3$ as a function of composition z . T_C (open circles), T_{CO} (open square), and T_N (open squares) represent ferromagnetic, charge-ordering, and antiferromagnetic transition temperatures, respectively. FM, AF-CE, and AF-A stand for ferromagnetic metallic, charge-ordered antiferromagnetic insulating (of the CE type), and antiferromagnetic states (perhaps of the A type), respectively. The hatched area represents the thermal hysteresis of T_{CO} and T_N . T_C , T_{CO} , and T_N determined under pressures (solid symbols) are also presented using a common scaling relation that $\Delta z = 0.04P$, P being in units of GPa.

ferromagnetic transition occurs and the system remains ferromagnetic metallic down to zero temperature.

B. Effect of an external magnetic field on antiferromagnetic states

An external magnetic field significantly affects these antiferromagnetic transitions via alignment of the local t_{2g} spins.^{2,13,14,18,19,23} For example, T_{CO} for $\text{Nd}_{1/2}\text{Sr}_{1/2}\text{MnO}_3$ ($z=0$) decreases with an increase of magnetic field and eventually the antiferromagnetic phase disappears above $\mu_0 H = 8$ T (in the field-cooling condition).¹³ The antiferromagnetic phase is expected to become more amenable to the magnetic field with an increase of W . We show in Fig. 5 the ρ - T curves (in both cooling and warming runs) under various magnetic fields for $(\text{Nd}_{1-z}\text{La}_z)_{1/2}\text{Sr}_{1/2}\text{MnO}_3$: (a) $z=0.4$ and (b) $z=0.5$. For $z=0.4$, the CO transition is suppressed by the field more effectively compared to $\text{Nd}_{1/2}\text{Sr}_{1/2}\text{MnO}_3$ ($z=0$) and extinguished readily above $\mu_0 H = 6$ T. On the other hand, the AF-A phase for $z=0.5$ is more robust against the field than the AF-CE state for $z=0.4$: The AF-A phase survives even above $\mu_0 H = 7$ T. This again implies that the magnetic structure of the AF-A phase is different in nature from that of the CE type.

V. CHARGE-ORDERING TRANSITIONS FOR $\text{Pr}_{1-x}\text{Ca}_x\text{MnO}_3$

A. Pressure control of CO transition

We exemplify in Fig. 6 the temperature dependence of resistivity (ρ , solid lines) and susceptibility ($\chi \equiv M/H$, filled

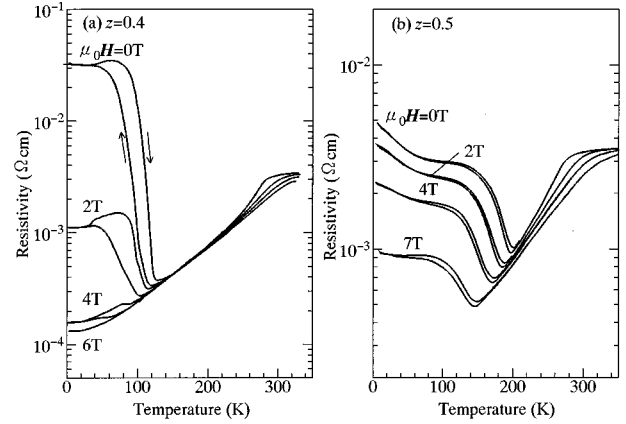


FIG. 5. Temperature dependence of resistivity for $(\text{Nd}_{1-z}\text{La}_z)_{1/2}\text{Sr}_{1/2}\text{MnO}_3$ crystals under external magnetic fields: (a) $z=0.4$ and (b) $z=0.5$.

circles) for the $\text{Pr}_{1-x}\text{Ca}_x\text{MnO}_3$ ($x=0.40$) crystal [see also the phase diagram shown in Fig. 1(c)]. An increase of ρ and a reduction of χ upon the CO transition indicates that the DE interaction is suppressed below T_{CO} due to localization of the carriers. (A thermal hysteresis upon the CO transition is shown for the resistivity curve.) With a further decrease of temperature, an antiferromagnetic spin ordering (CE type) occurs at $T_N = 170$ K (see Fig. 1).

The application of pressure and the resultant enhancement of the carrier itineracy suppress the CO transition also for $\text{Pr}_{1-x}\text{Ca}_x\text{MnO}_3$ with stronger CO instability. Figure 7 shows the ρ - T curves (in the heating run) under various pressures for (a) $x=0.50$, (b) 0.40, and (c) 0.35. The ρ - T curve shifts nearly rigidly toward the low-temperature side with external pressure. We adopted the inflection point of the ρ - T curve as T_{CO} (downward arrows in Fig. 7) and plotted in Fig. 8 values of $\Delta T_{CO}/T_{CO}^0$ against pressure, where $\Delta T_{CO} = T_{CO} - T_{CO}^0$ and T_{CO}^0 is the transition temperature at

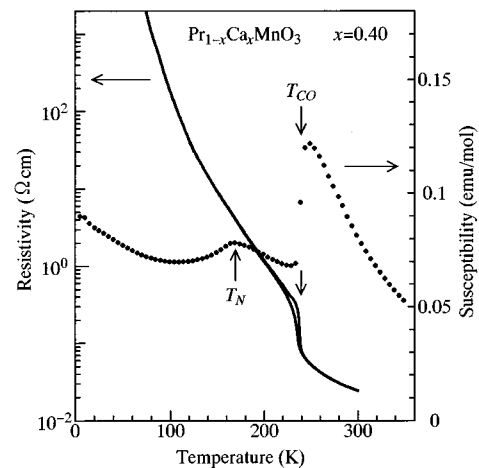


FIG. 6. Temperature dependence of resistivity (ρ) and susceptibility (χ) for $\text{Pr}_{1-x}\text{Ca}_x\text{MnO}_3$ ($x=0.40$) crystal. M was measured after cooling down to 5 K in the field of 3 T. T_{CO} and T_N stand for charge-ordering and antiferromagnetic transition temperatures, respectively.

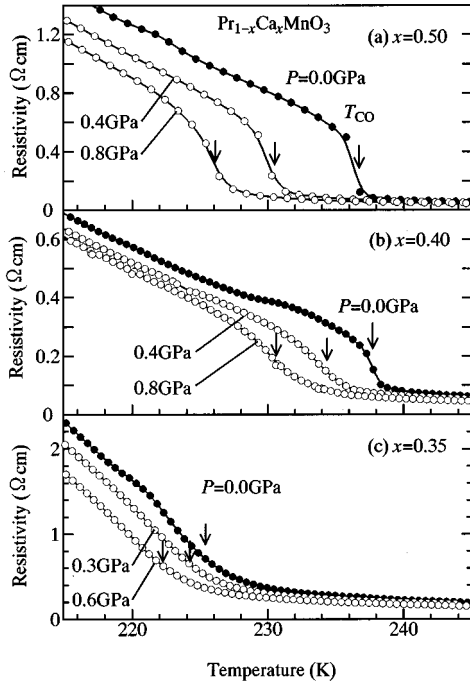


FIG. 7. Temperature dependence of resistivity for $\text{Pr}_{1-x}\text{Ca}_x\text{MnO}_3$ crystals under pressures ($x=0.50, 0.40,$ and 0.35). The resistivity was measured in the heating run. Arrows indicate the charge-ordering transitions.

ambient pressure. Open and filled symbols indicate T_{CO} for the heating and cooling runs, respectively. Solid lines are the results of a least-square fitting and hatched areas represent the thermal hysteresis. The absolute value of the pressure coefficient ($|d \ln T_{\text{CO}}/dP|$, slope of the line) is fairly small

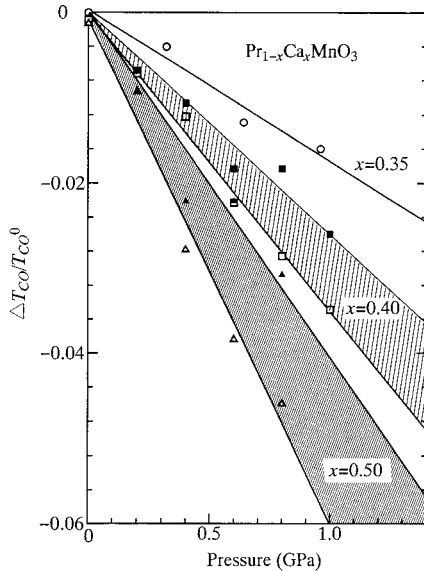


FIG. 8. Relative change of the charge-ordering temperature (T_{CO}) against pressure for $\text{Pr}_{1-x}\text{Ca}_x\text{MnO}_3$ crystals; $x=0.35$ (circles), 0.40 (squares), and 0.50 (triangles). Open and filled symbols are the values for the heating and cooling runs, respectively. Solid lines are the results of least-squares fitting and hatched areas represent the thermal hysteresis.

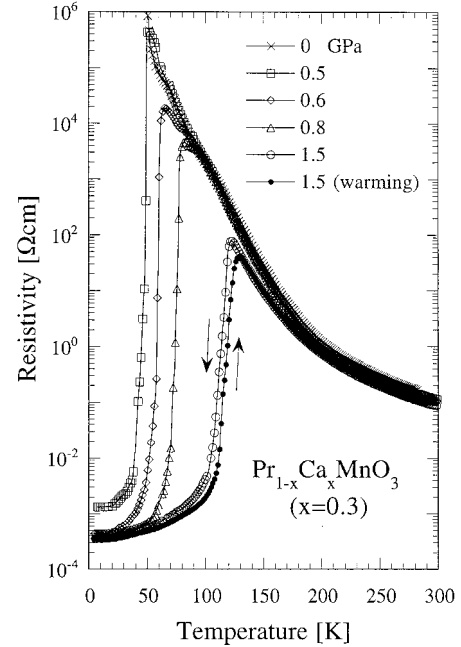


FIG. 9. Temperature dependence of resistivity for a $\text{Pr}_{0.7}\text{Ca}_{0.3}\text{MnO}_3$ ($x=0.30$) crystal under various pressures. Thermal hysteresis is exemplified for the runs at 1.5 GPa.

($\approx 0.02 \text{ GPa}^{-1}$) for $x=0.35$, but increases up to $0.04\text{--}0.06 \text{ GPa}^{-1}$ for $x=0.50$. The pressure-induced increase of the carrier itineracy, which tends to suppress the CO instability, seems to become more effective as x increases. We summarize in Table II the thusly obtained pressure coefficients together with T_{CO}^0 .

An even more drastic change of the transport property was found for the $\text{Pr}_{0.7}\text{Ca}_{0.3}\text{MnO}_3$ ($x=0.3$) crystal under pressures. Figure 9 shows the pressure dependence of the ρ - T curve for $x=0.3$. At ambient pressure, the ρ - T curve shows an insulating behavior and increases monotonically with a decrease of temperature. The compound shows the CO transition at $\approx 200 \text{ K}$ (Ref. 17) (see Fig. 1), though the corresponding anomaly is rather blurred in the ρ - T curve.²⁴ Under a pressure of 0.5 GPa, a steep drop of ρ by more than eight orders of magnitude is observed at $\approx 50 \text{ K}$. A similar pressure-induced IM transition was previously reported for $\text{Pr}_{0.7}\text{Ca}_{0.3}\text{MnO}_3$ ($x=0.3$) by Hwang *et al.*² This IM transition, which can be ascribed to the transition from a COI to a FM,^{18,19} accompanies thermal hysteresis (as exemplified for the 1.5-GPa data in Fig. 9) and hence perhaps some structural change. We tentatively adopted the maximum position of the ρ - T curve as the critical temperature (T_{IM}) for the IM transition and plotted T_{IM} in Fig. 10 against pressure. Open circles and squares are the values for the heating and cooling runs, respectively. T_{IM} suddenly emerges at $P \approx 0.5 \text{ GPa}$ and then gradually increases with pressure.

B. Comparison between the effects of pressure and magnetic field

In perovskite manganites, an external magnetic field has an effect similar to the application of pressure on the charge dynamics.²⁰ According to the DE theory,⁷ the effective trans-

TABLE II. Pressure and magnetic-field coefficients of the critical temperature (T_{CO}) for charge-ordering transition in $\text{Pr}_{1-x}\text{Ca}_x\text{MnO}_3$ crystals. T_{CO}^0 is the transition temperature at ambient pressure.

| x | Process | T_{CO}^0 (K) | $d \ln T_{\text{CO}}/dP$ (GPa^{-1}) | $d \ln T_{\text{CO}}/dH$ (T^{-1}) ^a | Ratio |
|------|---------|-----------------------|--|---|-------|
| 0.35 | | 225 | -0.018 | -0.0022 | 8.2 |
| 0.4 | heating | 238 | -0.035 | -0.002 ₈ | 12 |
| | cooling | 235 | -0.026 | -0.004 ₃ | 6 |
| | average | | -0.032 | -0.003 ₆ | 9 |
| 0.5 | heating | 237 | -0.059 | -0.006 ₈ | 9 |
| | cooling | 231 | -0.041 | -0.007 ₆ | 5 |
| | average | | -0.050 | -0.007 ₂ | 7 |

^aReference 19.

er interaction (t) of the e_g carrier is expressed by Eq. (1). An external pressure is considered to mainly affect the bare transfer interaction (t_0) via the volume contraction. By contrast, an external field forceably aligns the local spins ($\Delta\theta \rightarrow 0$) and increases t via a reduction of the spin scattering, which is also the major origin of the negative MR phenomena. The enhanced t under a magnetic field is expected to affect the CO transition as well. This was in fact demonstrated for a series of $\text{Pr}_{1-x}\text{Ca}_x\text{MnO}_3$ ($x=0.5, 0.4, 0.35$, and 0.4) crystals by Tomioka *et al.*¹⁹ Magnetic-field coefficients ($d \ln T_{\text{CO}}/dH$) estimated from the data presented in Ref. 19 are listed in Table II. The absolute magnitude of the coefficient ($|d \ln T_{\text{CO}}/dH|$) is x dependent and increases from $\approx 0.002 \text{ T}^{-1}$ for $x=0.35$ to $\approx 0.007\text{--}0.008 \text{ T}^{-1}$ for $x=0.50$. Nevertheless, the ratio of the pressure-to-field coefficient appears to be nearly x independent [$(d \ln T_{\text{CO}}/dP)/(d \ln T_{\text{CO}}/dH) \sim 7\text{--}9 \text{ T/GPa}$; see the averaged

values in Table II], indicating that the effects of pressure and magnetic field on the CO transition are almost equivalent.

$\text{Pr}_{0.7}\text{Ca}_{0.3}\text{MnO}_3$ ($x=0.3$) is known as a ‘‘colossal’’ MR compound and shows an IM transition at low temperatures under a magnetic field.^{2,18,19} We include in Fig. 10 values of T_{IM} under magnetic fields¹⁸ with filled circles (heating run) and squares (cooling run). A scaling relation holds between the field- and pressure-induced shifts of T_{IM} : The effect of the magnetic field of $\approx 6 \text{ T}$ is almost equivalent to that of the pressure of 1 GPa . Such a scaling relation suggests that the basic mechanisms for the pressure- and field-induced IM transitions are similar to each other. For the crystals with $x \geq 0.35$, no IM transition was observed under pressures up to 1.6 GPa . This is perhaps because the charge-ordered state becomes more robust as x approaches a commensurate value ($=\frac{1}{2}$). In fact, the critical field (H_C), which causes the IM transition at 5 K , increases from $H_C \approx 4 \text{ T}$ for $x=0.30$ to $\approx 9 \text{ T}$ for $x=0.40$.¹⁹

VI. CONCLUSION

We have investigated effects of chemical and external pressures, which both increase the one-electron bandwidth (W) of the e_g carriers, on the two types of charge-ordering transition. In the case of $\text{Nd}_{1-x}\text{Sr}_x\text{MnO}_3$ ($x=1/2$, type I), which shows a narrower one-electron e_g band than $\text{La}_{1-x}\text{Sr}_x\text{MnO}_3$, an insulating charge-ordered phase with antiferromagnetic CE-type spin structure sets in at $T_{\text{CO}}=158 \text{ K}$ below the Curie temperature $T_C=250 \text{ K}$. With an increase of W by partially replacing of Nd^{3+} ions with larger La^{3+} ions, the charge-ordered state is suppressed and finally disappears above $z=0.6$ for $(\text{Nd}_{1-z}\text{La}_z)_{1/2}\text{Sr}_{1/2}\text{MnO}_3$. We have found that in a narrow window of z ($0.4 \leq z \leq 0.6$) another type of antiferromagnetic (perhaps the A type) phase replaces the AF-CE state, as a possible consequence of the subtle balance between the competing interactions. For $\text{Pr}_{1-x}\text{Ca}_x\text{MnO}_3$ ($0.3 \leq x \leq 0.5$) with a further reduction of W , on the other hand, the CO state persists up to a relatively high temperature and no ferromagnetic metallic phase appears (type II). Similarly to the case of the type-I compound, the application of pressure suppresses the CO transition via pressure-enhanced carrier itineracy. For $\text{Pr}_{1-x}\text{Ca}_x\text{MnO}_3$ ($x=0.30$), however, the application of pressure induces the collapse of the charge-ordered state and

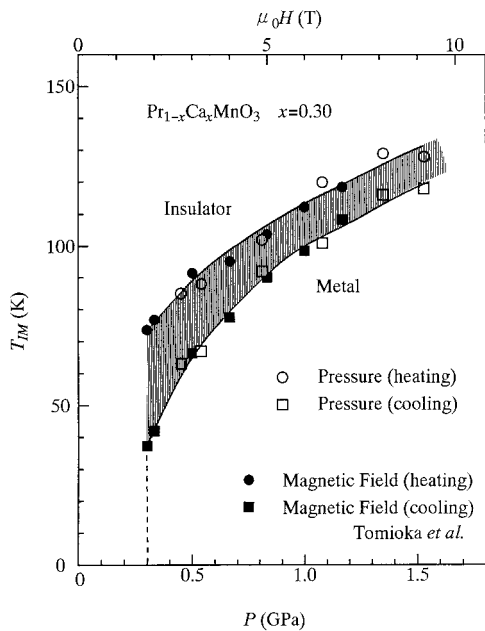


FIG. 10. Critical temperature (T_{IM}) for the insulator-to-metal transition as a function of pressure (open symbols) and magnetic field (filled symbols; cited from Ref. 18) for $\text{Pr}_{0.7}\text{Ca}_{0.3}\text{MnO}_3$ ($x=0.3$). Circles and squares represent the values for the heating and cooling runs, respectively, and the hatched area represents the thermal hysteresis.

produces a metallic phase from the low-temperature side. In other words, under pressure (≥ 0.5 GPa), as in a proper magnetic field, the FM phase is positioned at lower temperatures than T_{CO} , in sharp contrast to the type-I compound (e.g., $\text{Nd}_{1/2}\text{Sr}_{1/2}\text{MnO}_3$), in which the FM phase is located above T_{CO} .

ACKNOWLEDGMENTS

This work was supported by New Energy and Industrial Technology Development Organization and also by a Grant-In-Aid for Scientific Research from the Ministry of Education, Science and Culture, Japan.

*Present address: Center for Integrated Research in Science and Engineering, Nagoya University, Nagoya 464-01, Japan.

- ¹J. B. Torrance, P. Lacorre, A. I. Nazzal, E. J. Ansaldo, and Ch. Niedermeyer, *Phys. Rev. B* **45**, 8209 (1992).
- ²H. Y. Hwang, S.-W. Cheong, P. G. Radaelli, M. Marezio, and B. Batlogg, *Phys. Rev. Lett.* **75**, 914 (1995).
- ³H. Y. Hwang, T. T. M. Palstra, S.-W. Cheong, and B. Batlogg, *Phys. Rev. B* **52**, 15 046 (1995).
- ⁴X. Obradors, L. M. Paulius, M. B. Maple, J. B. Torrance, A. I. Nazzal, J. Fontcuberta, and X. Granados, *Phys. Rev. B* **47**, 12 353 (1993).
- ⁵P. L. Canfield, J. D. Thompson, S.-W. Cheong, and L. W. Rupp, *Phys. Rev. B* **47**, 12 357 (1993).
- ⁶Y. Moritomo, A. Asamitsu, and Y. Tokura, *Phys. Rev. B* **51**, 16 491 (1995).
- ⁷P. W. Anderson and H. Hasagawa, *Phys. Rev.* **100**, 675 (1955).
- ⁸P.-G. de Gennes, *Phys. Rev.* **118**, 141 (1960).
- ⁹Y. Tokura, A. Urushibara, Y. Moritomo, T. Arima, A. Asamitsu, G. Kido, and N. Furukawa, *J. Phys. Soc. Jpn.* **63**, 3931 (1994).
- ¹⁰A. Urushibara, Y. Moritomo, T. Arima, A. Asamitsu, G. Kido, and Y. Tokura, *Phys. Rev. B* **51**, 14 103 (1994).
- ¹¹N. Furukawa, *J. Phys. Soc. Jpn.* **63**, 3214 (1994).
- ¹²A. J. Millis, P. B. Littlewood, and B. I. Shraiman, *Phys. Rev. Lett.* **74**, 5144 (1994).
- ¹³H. Kuwahara, Y. Tomioka, A. Asamitsu, Y. Moritomo, and Y. Tokura, *Science* **270**, 961 (1995).
- ¹⁴Y. Tokura, H. Kuwahara, Y. Moritomo, Y. Tomioka, and A. Asamitsu, *Phys. Rev. Lett.* **22**, 3184 (1996).
- ¹⁵E. O. Wollan and W. C. Koehler, *Phys. Rev.* **100**, 545 (1951).
- ¹⁶E. Pollert, S. Krupicka, and E. Kuzmicova, *J. Phys. Chem. Solids* **43**, 1137 (1982); Z. Jirak, S. Krupicka, V. Nekvasil, Z. Simsa, M. Dlouha, and Z. Vratislav, *J. Magn. Magn. Mater.* **53**, 153 (1985).
- ¹⁷H. Yoshizawa, H. Kawano, Y. Tomioka, and Y. Tokura, *Phys. Rev. B* **52**, 13 145 (1995); Y. Yoshizawa, H. Kawano, Y. Tomioka, and Y. Tokura, *J. Phys. Soc. Jpn.* **65**, 1043 (1996).
- ¹⁸Y. Tomioka, A. Asamitsu, Y. Moritomo, and Y. Tokura, *J. Phys. Soc. Jpn.* **64**, 3624 (1995).
- ¹⁹Y. Tomioka, A. Asamitsu, H. Kuwahara, Y. Moritomo, and Y. Tokura, *Phys. Rev. B* **53**, R1689 (1996).
- ²⁰Y. Moritomo, A. Asamitsu, and Y. Tokura, *Phys. Rev. B* **51**, 16 491 (1995).
- ²¹R. C. Vickery and A. Klann, *J. Chem. Phys.* **37**, 1161 (1957).
- ²²H. Kawano, R. Kajimoto, H. Yoshizawa, Y. Tomioka, H. Kuwahara, and Y. Tokura, *Phys. Rev. B* (to be published).
- ²³Y. Tomioka, A. Asamitsu, Y. Moritomo, H. Kuwahara, and Y. Tokura, *Phys. Rev. Lett.* **74**, 5108 (1995).
- ²⁴A sign of the CO transition is seen in the ρ - T curve as an increase of the activation energy [proportional to $d(\ln\rho)/d(T^{-1})$] around ~ 200 K. The anomaly remains even under pressure of 1.5 GPa.